Article

Multi-Temporal and Multiscale Satellite Remote Sensing Imagery Analysis for Detecting Pasture Area Changes after Grazing Cessation Due to the Fukushima Daiichi Nuclear Disaster

Muxiye Muxiye and Chinatsu Yonezawa *

Graduate School of Agricultural Science, Tohoku University, 468-1 Aramaki Aza Aoba, Aoba-ku, Sendai 980-8572, Miyagi, Japan; muxiye.r6@dc.tohoku.ac.jp
* Correspondence: chinatsu.yonezawa.e7@tohoku.ac.jp

Abstract: Despite advancements in remote sensing applications for grassland management, studies following the 2011 Fukushima Daiichi nuclear disaster have often been constrained by limited satellite imagery with insufficient focus on pasture changes. Utilizing different resolutions of optical satellite data is essential for monitoring spatiotemporal changes in grasslands. High resolutions provide detailed spatial information, whereas medium-resolution satellites offer an increased frequency and wider availability over time. This study had two objectives. First, we investigated the temporal changes in a mountainous pasture in Japan from 2007 to 2022 using high-resolution data from QuickBird, WorldView-2, and SPOT-6/7, along with readily available medium-resolution data from Sentinel-2 and Landsat-5/7/8. Second, we assessed the efficacy of different satellite image resolutions in capturing these changes. Grazing ceased in the target area after the 2011 Fukushima Daiichi nuclear accident owing to radiation. We categorized the images as grasses, broadleaf trees, and conifers. The results showed a 36% decline using high-resolution satellite image analysis and 35% using Landsat image analysis in the unused pasture area since grazing suspension in 2011, transitioning primarily to broadleaf trees, and relative stabilization by 2018. Tree encroachment was prominent at the eastern site, which has a lower elevation and steeper slope facing north, east, and south. WorldView-2 consistently outperformed Landsat-8 in accuracy. Landsat-8's classification variation impedes its ability to capture subtle distinctions, particularly in zones with overlapping or neighboring land covers. However, Landsat effectively detected area reductions, similar to high-resolution satellites. Combining high- and medium-resolution satellite data leverages their respective strengths, compensates for their individual limitations, and provides a holistic perspective for analysis and decision-making.

Keywords: pasture area; land use and land cover classification; time series analysis

1. Introduction

Grasslands are among the most important ecosystems on Earth, covering 31–43% of the world's total land area [1]. They support rich biodiversity, provide valuable ecosystem services, and are widely used for grazing livestock [1,2]. However, grasslands face degradation worldwide owing to both underuse and overuse [2,3]. Grazing intensity, historical conditions, and geographical location all play important roles in shaping vegetation diversity and productivity in grassland ecosystems [4–6]. In Japan, grasslands account for 1% or less of the national land, a significant decrease from the past [7]. This decline, attributed to reduced human activity, has led to diminishing biodiversity and is considered as the "Second crisis", one of the four factors contributing to the decline in Japan's biodiversity [8]. Given the country's humid, warm-temperate environment, which favors spontaneous forest growth, human intervention is crucial for grassland maintenance [9,10]. Considering the importance of grasslands, it is critical to monitor changes over time. Remote sensing technology provides an effective means of detecting and tracking grassland changes [11] and

can contribute to the development of effective management and conservation strategies for critical ecosystems [12]. Satellite imagery and aerial photography provide comprehensive data on vegetation fluctuation over time, even in areas that are difficult to access.

Time-series analysis using optical satellite data is a pivotal tool for assessing spatiotemporal changes in grasslands. This approach primarily relies on detecting temporal variances in grassland reflectance properties through the analysis of spectral bands or vegetation indices, which can reveal changes associated with plant phenology or different management practices. Globally, optical imagery has been extensively utilized to monitor grassland management and use intensity over varying temporal scales. For example, in southern Bavaria, RapidEye data were used to differentiate between extensive and intensive grassland management through time series analysis [13]. Similarly, Landsat imagery in Switzerland was used to distinguish between mowing and grazing practices [14]. In Slovakia, research using vegetation indices such as EVI and NDVI showcased the capability of these techniques in differentiating between cut and uncut meadows [15]. In Australia, the correlation between NDVI and biomass was explored, evidencing its relevance to the grazing industry [16]. Sentinel-2 data were instrumental in Germany's efforts to quantify grassland management parameters like grazing intensity and mowing frequency [17]. Furthermore, the application of optical satellite data in mapping vegetation distribution has been evident in various studies. For instance, in Yellowstone National Park, the spectral features of optical multispectral data were utilized to map the distribution of vegetation [18]. In Italy's Gran Paradiso National Park, high-resolution remote sensing data were used to predict mountain grassland distribution [19]. Additionally, the amalgamation of PALSAR data with Landsat time series imagery in the U.S. Southern Great Plains facilitated the tracking of tree encroachment into grasslands [20]. Also, in the Eurasian steppe, multisource remote sensing images were employed to observe the encroachment of woody vegetation into grasslands due to warming trends [21].

The application of classification techniques using multi-temporal satellite observations plays a crucial role in this analytic framework. There are several types of optical satellite image data, each with different levels of spatial resolution, including very high (<5 m), high (5–9.9 m), medium (10–39.9 m), moderate (40–249.9 m), and low (250 m–1.5 km) [22]. These data differ in resolution and frequency of observations, with high-resolution satellite imagery capturing detailed information about the Earth's surface. On the one hand, high-resolution satellite data are often provided at a fee. On the other hand, although they offer less detail, medium-resolution satellites have the advantages of increased frequency and unrestricted access spanning several decades. These satellite data, each with its unique advantages, create a trade-off dilemma: spatial resolution, which determines the detail of observed phenomena, versus temporal resolution, dictating how frequently these phenomena are observed. Evaluating the advantages and limitations of each resolution type for various research areas helps ensure that the selected data source aligns with research objectives and yields pertinent and precise results. Through the comparison and combination of datasets with varying resolutions, researchers can achieve a broader perspective on environmental phenomena and their dynamics, leading to well-rounded and sound conclusions. Therefore, for the sustained monitoring of grasslands, where both detailed and long-term observations are important, utilizing the capabilities of different resolution datasets is of significant value. Therefore, long-term monitoring of grasslands should utilize these various-resolution datasets.

The purpose of this study was to Investigate the changes in pasture areas where grazing was suspended following the Fukushima Daiichi nuclear disaster caused by the Great East Japan Earthquake on 11 March 2011, using multi-spatial-resolution optical satellite data. This disaster led to widespread radioactive material contamination in eastern Japan [23], resulting in a temporary suspension of grazing activities in several prefectures, including Iwate, Miyagi, Fukushima, Tochigi, and Gunma [24]. Given that grasslands account for less than 1% of the national land area of Japan [7], understanding the ecological impacts of grazing suspension is crucial. The warm and humid climate, favoring forest

growth [9,10], might make these regions susceptible to woody encroachment, potentially leading to significant shifts in ecosystem structure and function. These changes in land cover could be influenced by topographical factors. Optical remote sensing technology has previously demonstrated its efficacy in monitoring land-use changes caused by the aforementioned disaster. For instance, in a study by Harada et al. [25], researchers produced a detailed Land Use and Land Cover map of a district in the Tohoku region after the 2011 East Japan earthquake for the 2013–2015 period using Land-sat-8 OLI data. Their findings revealed significant land transformations from rice paddies to grasslands along the tsunami-affected coast and within the evacuation zone. Ishihara and Tadono [26] utilized 2013 Terra/MODIS data to classify land cover types across eastern Japan, particularly focusing on the Tohoku area. Their observations highlighted drastic vegetation changes following the 2011 Great Eastern Japan Earthquake. Additionally, Hirayama et al. [27] employed RapidEye satellite images to generate land cover maps of a district in Tohoku affected by the 2011 earthquake and tsunami for the years 2010, 2011, 2012, and 2016. However, these studies primarily relied on limited satellite imagery with insufficient focus on pasture changes. Thus, to achieve a comprehensive understanding and continuous tracking of land cover alterations, particularly in suspended pasture zones, it is imperative to harness multi-temporal and multiscale satellite imagery that offers both high spatial and temporal resolutions. This approach, by combining the spatial detail of high-resolution images with the temporal breadth of medium-resolution data, is particularly crucial for a detailed analysis of pasture changes. Specifically, we (1) compared and evaluated the effectiveness of freely accessible medium-resolution image data against high-resolution data in quantifying pasture area changes and (2) clarified the impact of cattle grazing cessation on pastures.

2. Materials and Methods

2.1. Study Area

The study area was a mountainous pasture in the Integrated Terrestrial Field Station of Tohoku University, located in Osaki City, Miyagi Prefecture, Japan (Figure 1). Originally a military horse breeding facility established in 1888, the field station transitioned in 1949 to serve as a farm and practice forest affiliated with Tohoku University's Faculty of Agriculture. The Field Station encompasses a 2215 ha territory with a well-distributed mix of forest lands (1719 ha), grasslands (429 ha), and farmlands (19 ha). The forests are primarily composed of *Cryptomeria japonica* plantations and temperate deciduous broadleaf forests that include species such as *Fagus crenata* Blume and *Quercus crispula* Blume var. *crispula*. It is located 150 km northwest of the Fukushima Daiichi Nuclear Power Station. Since 2011, grazing has been suspended because of the dispersal of radioactive substances by the Nuclear Power Station accident. The diverse topography of the area, characterized by varied terrains, wild forests, and grasses, has made radioactive decontamination efforts especially difficult. To date, initiatives to undertake tilling decontamination for radioactive remediation have not proceeded. The prevailing climate in this region is temperate, as evidenced by meteorological data collected by the Japan Meteorological Agency at the Kawatabi meteorological station [28]. This station is located 3 km south of the study area and 170 m above sea level. The data show a mean annual rainfall of 1643 mm, an average temperature of 10.4 °C, and 1584.8 annual sunshine hours. Given the location of the study area, it is likely to be cooler than suggested by the station data.
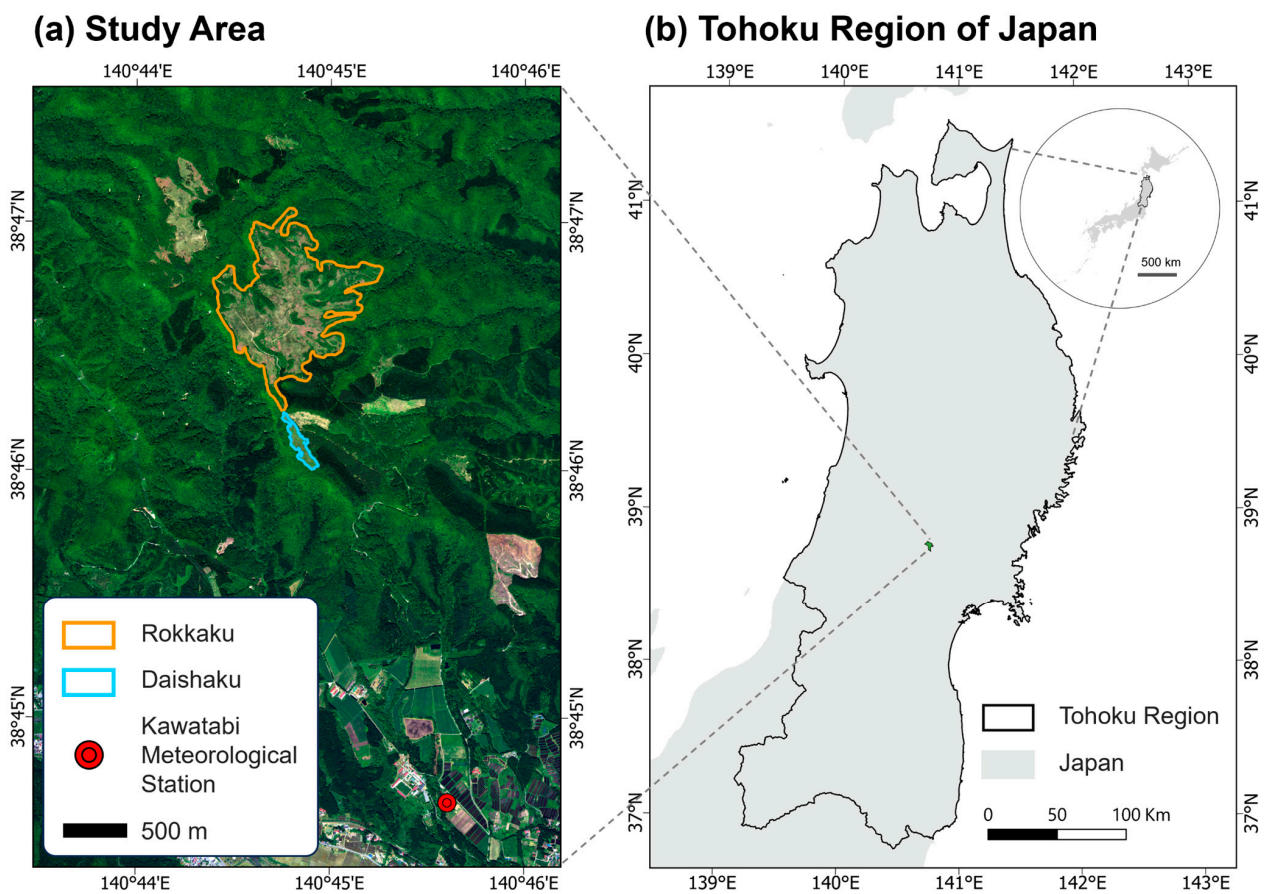
Figure 1. Geographic position of the study area. (**a**) True-color RGB (R: band 5; G: band 3; B: band 2) visualization of the study area as captured by the WorldView-2 satellite on May 26, 2018. The pasture outlined by the yellow line signifies the Rokkaku pasture, the blue line represents the Daishaku pasture, and the red circle indicates the location of Kawatabi Meteorological Station. (**b**) The specific location of the study area within the Tohoku region of Japan.

This study focused on the Rokkaku pasture, which had an area measuring 66.1 ha in 2007 [29] During the period leading up to this disaster, the pasture was used for Japanese Black and Japanese Shorthorn cattle grazing without mineral fertilizers. Located in alpine surroundings, the elevation of the Rokkaku pasture varies from 483 to 621 m. The landscape consists of diverse hillslopes, with a mean slope of 10.8°, ranging from 0.2° to 31.4°. The predominant grass species include *Anthoxanthum odoratum* L., *Carex albata* Boott, *Agrostis alba* L., *Poa pratensis* L., *Dactylis glomerata* L., *Lolium perenne* L., and *Trifolium repens* L. In addition, the Daishaku pasture, which was continuously grazed for experimental studies using cattle not intended for shipment after the disaster, was also studied for comparative purposes. On 30 May 2019, a field survey was conducted in the Rokkaku pasture to assess its state and compare it with the classification results of the previous year.

2.2. Data and Methods

2.2.1. Multiscale Optical Satellite Images for Classification

As shown in Table 1, a combination of high-resolution and medium-resolution satellite imagery from diverse satellites over varied time frames was utilized. We collected high-resolution satellite data from QuickBird (multispectral resolution 2.4 m) on 19 July 2012, Worldview-2 (multispectral resolution 1.8 m) on 20 May 2017, 26 May 2018, and 20 November 2021, and SPOT 6/7 (multispectral resolution 6 m) on 26 September 2014, 1 October 2015, 25 May 2019, and 4 May 2022. These high-resolution images with detailed spatial observations were able to capture intricate ground features. However, obtaining a

continuous series of these images for extended durations was challenging, as mountain pastures like our study area are frequently obscured by clouds. Therefore, we collected high-resolution images free from cloud interference, even if that required using different sensors and dates. In contrast, medium-resolution images, especially those from the Landsat series, provided expansive temporal insights. We utilized multi-temporal Landsat-5/7/8 images with a spatial resolution of 30 m, and cloud-free images observed from May to August 2007–2022 were selected for analysis. Data collection during May and June was informed not solely by the prevalent cloud cover from August through April but also by the study area's peak growing season, spanning from late spring to early summer. Additionally, we used Sentinel-2 images with a resolution of 10 m for the period from May to July between 2017 and 2022, which has a higher resolution than that of Landsat data and can be used free of charge, enabling us to obtain more detailed information. We utilized high-resolution images for a detailed spatial perspective—especially for ground intricacies—while relying on medium-resolution images to observe longer-term trends and changes. By combining these satellite data, we determined pasture changes more accurately. We used 10-m mesh digital elevation model (DEM) data updated by the Geospatial Information Authority of Japan on 1 October 2016. When creating land cover classification maps, we referred to field survey data and images from Google Earth as well as the vegetation map of Miyagi Prefecture Forest Information Provision System updated on 1 April 2015.

Table 1. Observation dates and details of multi-sensor satellite imagery.

Data	High-Resolution			Free Source			
	WorldView-2	QuickBird	SPOT-6/7	Sentinel-2	Landsat-5	Landsat-7	Landsat-8
Spatial Resolution (Multispectral)	1.8 m	2.4 m	6 m	10 m	30 m	30 m	30 m
Spectral Range in nm (no. of bands)	400–1040 (8)	450–900 (4)	455–890 (4)	455–885 (4)	460–900 (4)	460–900 (4)	433–885 (4)
Observation Dates	20 May 2017 26 May 2018 20 November 2021	19 July 2012	26 September 2014 1 October 2015 25 May 2019 4 May 2022	7 July 2017 2 June 2018 23 May 2019 2 May 2020 11 June 2021 2 May 2022	13 June 2007 2 June 2009 8 August 2010 8 June 2011	22 May 2008 2 June 2012 5 June 2013	31 May 2014 2 May 2015 20 May 2016 23 May 2017 26 May 2018 14 June 2019 31 May 2020 18 May 2021 5 May 2022

2.2.2. Optical Imagery Preprocessing

All high-resolution images were radiometrically corrected for distortions caused by factors such as sensors, sunlight, and atmosphere [30]. Calibration was undertaken for all multispectral bands using "Reflectance" as the specified type, transforming Digital Numbers into ground reflectance values. We selected this reflectance calibration because it provided a consistent and physically interpretable metric, ensuring uniformity in analysis across diverse datasets, irrespective of variations in acquisition timings or sensor differences. We performed ortho-rectification using an RPC file and a 10-m mesh DEM from the Geospatial Information Authority of Japan to correct for distortions caused by the terrain. For Landsat-5/7/8, we used Collection 2 Level-2 data that had already undergone both geometric and radiometric corrections. However, Landsat-7 images after 2003 contained stripe-shaped data gaps due to equipment malfunctions; therefore, we conducted gap-fill processing [31] for each band. For Sentinel-2, we used Level-1C orthorectified data and performed the same radiometric correction as that applied to the high-resolution imagery as a preprocessing step. For all the satellite images, we generated a pan-sharpened image that combined a high-resolution panchromatic image with a low-resolution multispectral image for visual interpretation.

2.2.3. Land Cover Classification

Vegetation was grouped into three categories (grasses, broadleaf trees, and coniferous trees) in multispectral images using the pixels-based maximum likelihood method. To differentiate these classes, we relied on their distinct spectral signatures. Grasslands, with their mix of photosynthetic vegetation and soil, differ spectrally from forests, which combine photosynthetic and woody vegetation, soils, and shadows [32]. Previous studies have highlighted the importance of visible wavelengths in differentiating tree types [33] notably, conifers, attributed to their reduced photosynthetic activity in the blue band [34]. We evaluated the classification accuracy using a confusion matrix. To examine the temporal changes, we compared the pasture areas extracted from the land-cover classification maps of the two test sites. To investigate the spatial variations in vegetation, we generated a change map using classification maps derived from high-resolution satellite images captured in 2012, 2015, 2018, and 2021. For consistency in our spatial analysis, we standardized all four classification images to a resolution of 6 m, given that the lowest spatial resolution in the high-resolution data was from SPOT. Subsequently, a pixel-by-pixel comparison of the two time points was conducted. The spatial structure indices calculated in this study were the area occupied by each vegetation category along with their respective percentages. Analyzing the proportionate distribution of each category, we were able to estimate the variations in the expanse of each type of vegetation over time. We then categorized the transformations observed during the 2012–2015, 2015–2018, 2018–2021, and 2012–2021 periods into three categories: changes from grasses to broadleaf trees, changes from grasses to coniferous trees, and no-change regions.

2.2.4. Topographic Map

To analyze the relationship between topography and vegetation change, we computed parameters such as slope and aspect using DEM data (10-m resolution). Three distinct maps—elevation, slope, and aspect—were generated.

2.3. Data Analysis
2.3.1. Temporal Change Trend Analysis of the Pasture Area

We evaluated the temporal variations in the pasture area using Theil–Sen median slope trend analysis. This assessment was based on area calculations derived from three different sources, each evaluated independently: (1) high-resolution satellite, (2) Landsat, and (3) Sentinel-2 imagery. The robustness of this method, as initially proposed by Theil [35] and later refined by Sen [36], allows the mitigation of outlier impacts, thus yielding a reliable representation of the intrinsic trend within the dataset. To identify any discernible increase, decrease, or stability in pasture area trends over the study period, we employed the Mann–Kendall significance test [37,38]. The Mann–Kendall test, a nonparametric method, is often employed to ascertain the presence of a monotonic trend within a time series, thereby, serving as an authoritative approach for substantiating the significance of the Theil–Sen slope.

2.3.2. Spatial Changes in the Pasture

To examine the statistical relationship between topographic characteristics (elevation, slope, and aspect) and vegetation change in the study area, we utilized the change map from the 2012–2021 period, resampled to a 10-m resolution to match the topographic maps. Vegetation changes were categorized into three groups: no change (NC), grasses to coniferous trees (GC), and grasses to broadleaf trees (GB). We then employed a non-parametric statistical method using the Kruskal–Wallis H test [39], followed by Dunn's post-hoc test [40]. The Kruskal–Wallis H test is useful when dealing with data that do not follow a normal distribution, such as topographic characteristics, or when the sample size is relatively small, as in the GC group. Dunn's post-hoc test, on the other hand, was used to make pairwise comparisons between groups if the Kruskal–Wallis H test determined that differences existed.

3. Results

3.1. Accuracy Verification for Classification

Table 2 lists the overall classification accuracy (OA) and Kappa coefficients of the multi-temporal data. In the examination of the three satellite data sources—high-resolution, Sentinel-2, and Landsat-5/7/8—the OA and Kappa coefficients suggest that high-resolution and Sentinel-2 data exhibited slightly higher classification accuracy. Specifically, high-resolution images had a mean OA of 0.93, spanning from 0.88 to 0.95. Sentinel-2 presented a mean OA of 0.93, closely aligned with that of high-resolution images, ranging from 0.90 to 0.95. Meanwhile, Landsat-5/7/8 demonstrated a slightly lower average OA of 0.90, with values between 0.84 and 0.95. In the context of the mean Kappa coefficient, high-resolution images reported a value of 0.88, followed by the Sentinel-2 and Landsat-5/7/8 coefficients, at 0.87 and 0.83, respectively.

Table 2. Overall classification accuracy (OA) assessment and Kappa coefficients of multi-temporal data.

High-Resolution			Sentinel-2			Landsat-5/7/8					
Date	OA	Kappa	Date	OA	Kappa	Date	OA	Kappa	Date	OA	Kappa
19 July 2012	0.95	0.92	7 July 2017	0.94	0.90	13 June 2007	0.91	0.86	2 May 2015	0.92	0.86
26 September 2014	0.91	0.87	2 June 2018	0.92	0.85	22 May 2008	0.88	0.80	20 May 2016	0.95	0.91
1 October 2015	0.88	0.81	23 May 2019	0.95	0.90	2 June 2009	0.87	0.80	23 May 2017	0.87	0.77
20 May 2017	0.94	0.90	2 May 2020	0.93	0.87	8 August 2010	0.86	0.75	26 May 2018	0.93	0.87
26 May 2018	0.95	0.92	11 June 2021	0.94	0.89	8 June 2011	0.90	0.83	14 June 2019	0.94	0.89
25 May 2019	0.95	0.90	2 May 2022	0.90	0.82	2 June 2012	0.85	0.76	31 May 2020	0.95	0.89
20 November 2021	0.93	0.87				5 June 2013	0.84	0.73	18 May 2021	0.92	0.84
4 May 2022	0.93	0.88				31 May 2014	0.91	0.85	5 May 2022	0.95	0.90

Figure 2 shows a comparison of the vegetation classification maps derived from WorldView-2 and Landsat-8, both captured on 26 May 2018. With its finer 1.8-m resolution, WorldView-2 consistently outperformed Landsat-8, which offers a 30-m resolution in terms of OA and Kappa coefficient. WorldView-2 exhibited a Kappa coefficient of 0.92, in contrast to the 0.87 achieved by Landsat-8. However, it is worth noting the noise in the classification of high-resolution satellite images. For the "grasses" classification, WorldView-2 was superior to Landsat-8 in both user and producer accuracies. The observed classification variances in Landsat-8 can likely be attributed to its coarser 30-m resolution, which could impede its ability to capture subtle distinctions in the imagery, especially in zones with overlapping or neighboring land cover types. Regarding calculated pasture areas, WorldView-2, with a 1.8-m resolution, estimated the area of the Rokkaku pasture to be 41.9 ha and the Daishaku pasture to be 2.7 ha. In contrast, Landsat-8, with a 30-m resolution, estimated the same pastures to be 44.6 and 2.8 ha, respectively. A variance of 2.7 ha in the Rokkaku pasture was observed between the two satellites. Despite the disparity in the 1.8-m resolution of WorldView-2 versus the 30-m resolution of Landsat-8, both satellites provided similar area measurements, suggesting WorldView-2's detailed imaging capability and the overall reliability of both satellites.

3.2. Temporal Changes in Pasture Area

Figure 3 illustrates the temporal variation in pasture areas, as examined by high-resolution satellite, Landsat, and Sentinel-2 images. The statistical significance of these variations was determined using the Mann–Kendall test.

3.2.1. Temporal Changes in Rokkaku Pasture (Grazing Cease)
Temporal Variation before the 2011 Earthquake

Previous data from 24 July 2007, indicated that the Rokkaku pasture area was 66.1 ha [29]. Comparing the data from 2007 with the calculations from 2012 using high-resolution satellite imagery, we observed no significant area changes in the pasture before the 2011 earthquake. Examining Landsat-5/7/8 images obtained from May to August from 2007 to 2011, it is evident that the Rokkaku pasture area remained relatively stable ($p = 0.6$), fluctuating between 67.2 and 68.5 ha.
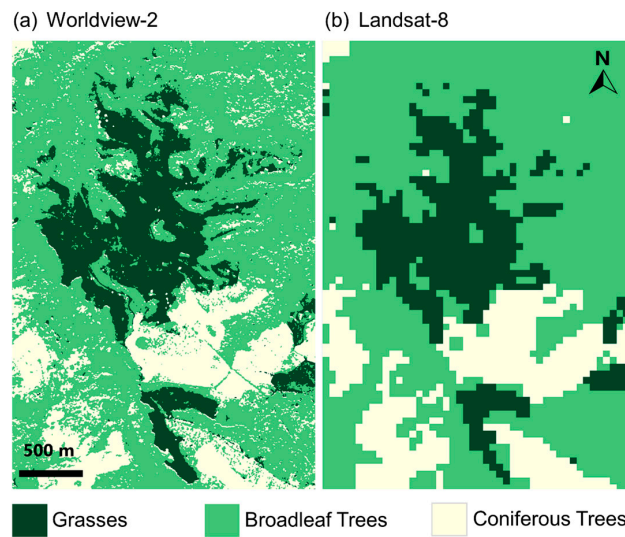
Figure 2. Vegetation classification maps derived from (**a**) WorldView-2 and (**b**) Landsat-8, both captured on 26 May 2018. The classifications are divided into three categories: grasses, broadleaf trees, and coniferous trees.
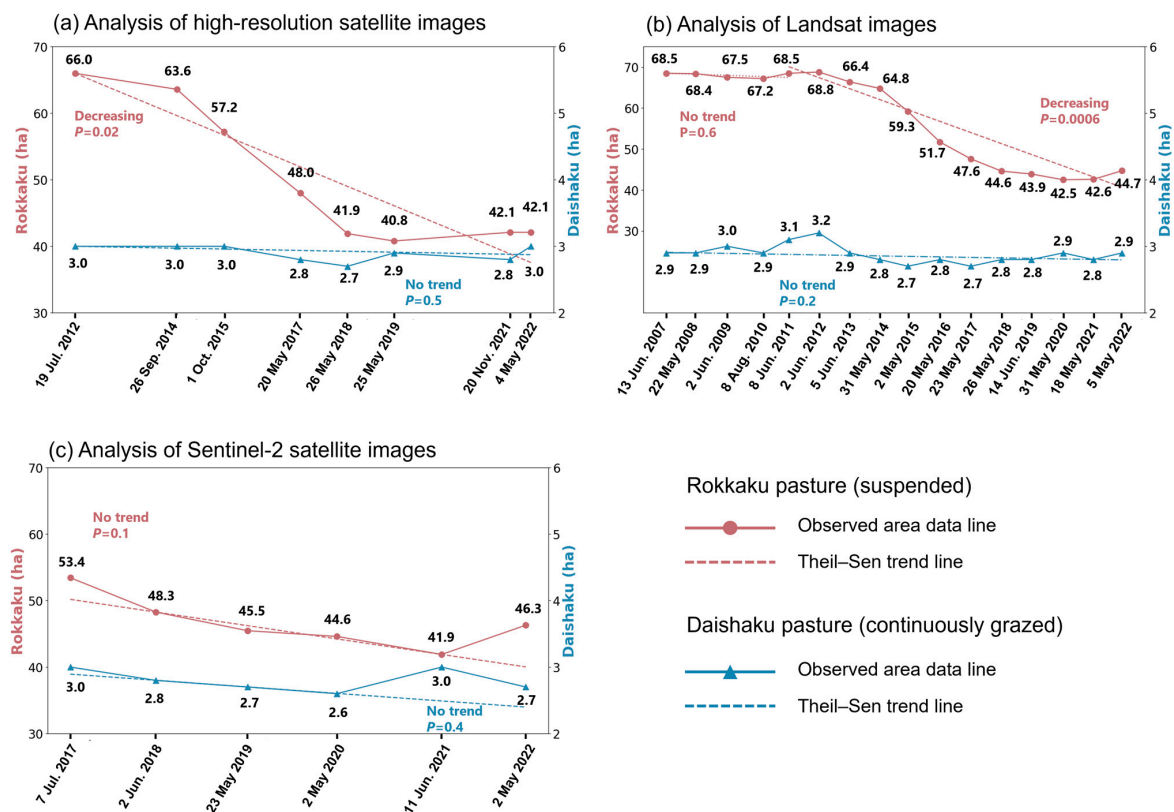

Figure 3. Temporal variation in pasture area using satellite imagery. (**a**) High-resolution satellite images, (**b**) Landsat images, and (**c**) Sentinel-2 images. Each plot's horizontal axis represents the timeline of satellite observations, whereas the dual vertical axes denote the respective areas of the Rokkaku (left) and Daishaku (right) pastures, quantified in hectares. The red solid line with circular markers is the observed area data for the Rokkaku pasture, whereas the red dashed line presents its Theil–Sen trend line. Similarly, the Daishaku pasture's observed area data are represented by the blue solid line with triangle markers, with its Theil–Sen trend line presented as the blue dashed line. *p*-values were determined using the Mann–Kendall significance test. $p \geq 0.05$ indicates no trend, whereas $p < 0.05$ indicates a statistically significant increase or decrease.

Temporal Variation after the 2011 Earthquake

After 2011, high-resolution satellite imagery revealed a notable decrease in the Rokkaku pasture area, from 66.0 ha in 2012 to 42.1 ha in 2022, signifying a significant approximate reduction of 36%, with $p < 0.05$ (Figure 3a). Landsat-5/7/8 satellite images from 2011 to 2022 showed a steady decline in the Rokkaku pasture, culminating in a significant approximate total reduction of 35% (Figure 3b; $p < 0.001$). These results align closely with those derived from high-resolution imagery. Analyzing Sentinel-2 satellite images captured between May and July from 2017 to 2022 revealed decreasing fluctuations in the Rokkaku pasture area: 53.4 ha in 2017, 48.3 ha in 2018, 45.4 ha in 2019, 44.6 ha in 2020, 41.9 ha in 2021, and 46.3 ha in 2022. However, no statistically significant changes were observed during this period (Figure 3c, $p = 0.1$).

3.2.2. Temporal Changes in Daishaku Pasture (Grazing Continuation)

Conversely, the Daishaku pasture, which was subjected to continuous grazing, showed notable stability without any significant changes over time. High-resolution satellite imagery indicated that the extent of the Daishaku pasture varied marginally between 2.7 and 3.0 ha, with no statistical significance ($p = 0.5$). Furthermore, data from the Landsat-5/7/8 satellite images echoed this finding, revealing that the area of this pasture fluctuated between 2.7 and 3.2 ha during the 2007–2022 period, without any significant deviations ($p = 0.2$). Similarly, Sentinel-2 satellite imagery recorded variations in the pasture area, ranging between 2.6 and 3.0 ha, with no significant differences ($p = 0.4$).

3.3. Spatial Changes in Pasture Area by High-Resolution Imagery

Figure 4 illustrates the dynamic shifts in vegetation within the Rokkaku pasture over three distinct periods: 2012–2015, 2015–2018, and 2018–2021. Included are true-color RGB images from four specific dates: 19 July 2012 (QuickBird, R: band 3; G: band 2; B: band 1), 1 October 2015 (SPOT-7, R: band 3; G: band 2; B: band 1), 26 May 2018 (WorldView-2, R: band 5; G: band 3; B: band 2), and 20 November 2021 (WorldView-2, R: band 5; G: band 3; B: band 2), which serve to visually interpret vegetation transitions. Denser green tones represent forested areas, while lighter shades represent pastures. Despite seasonal variations in color tones, a progression of encroachment of forested areas was observed. A significant transition from grasses to treed areas was predominantly observed along the constricted northern boundary (Figure 4b). This change occurred primarily during the 2015–2018 period. Tree encroachment was also notably observed within the eastern side regions, with the main shift occurring within the same period, i.e., 2015–2018 (Figure 4c). An exclusively narrow segment on the southern edge underwent a complete transformation into a treed area, with the western portion primarily changing from 2012 to 2015 and the remaining area undergoing transformation between 2015 and 2018 (Figure 4d). Moreover, tree encroachment was observed in the northwestern part of Region 3 (Figure 4d), mainly in 2015–2018.

Unused pasture decreased since the voluntary grazing suspension in 2011, changing to a forest mainly dominated by broadleaf trees (Figure 5). In the 2012–2015 period, 12.6% of the study area transitioned from grasses to broadleaf trees. The transition rate increased significantly to 18.4% between 2015 and 2018. However, a decline was observed from 2018 to 2021, with a 5.8% transition from grasses to broadleaf forests. Overall, from 2012 to 2021, a considerable 24.5% transitioned from grasses to broadleaf trees. A shift from GC was significantly less prevalent.
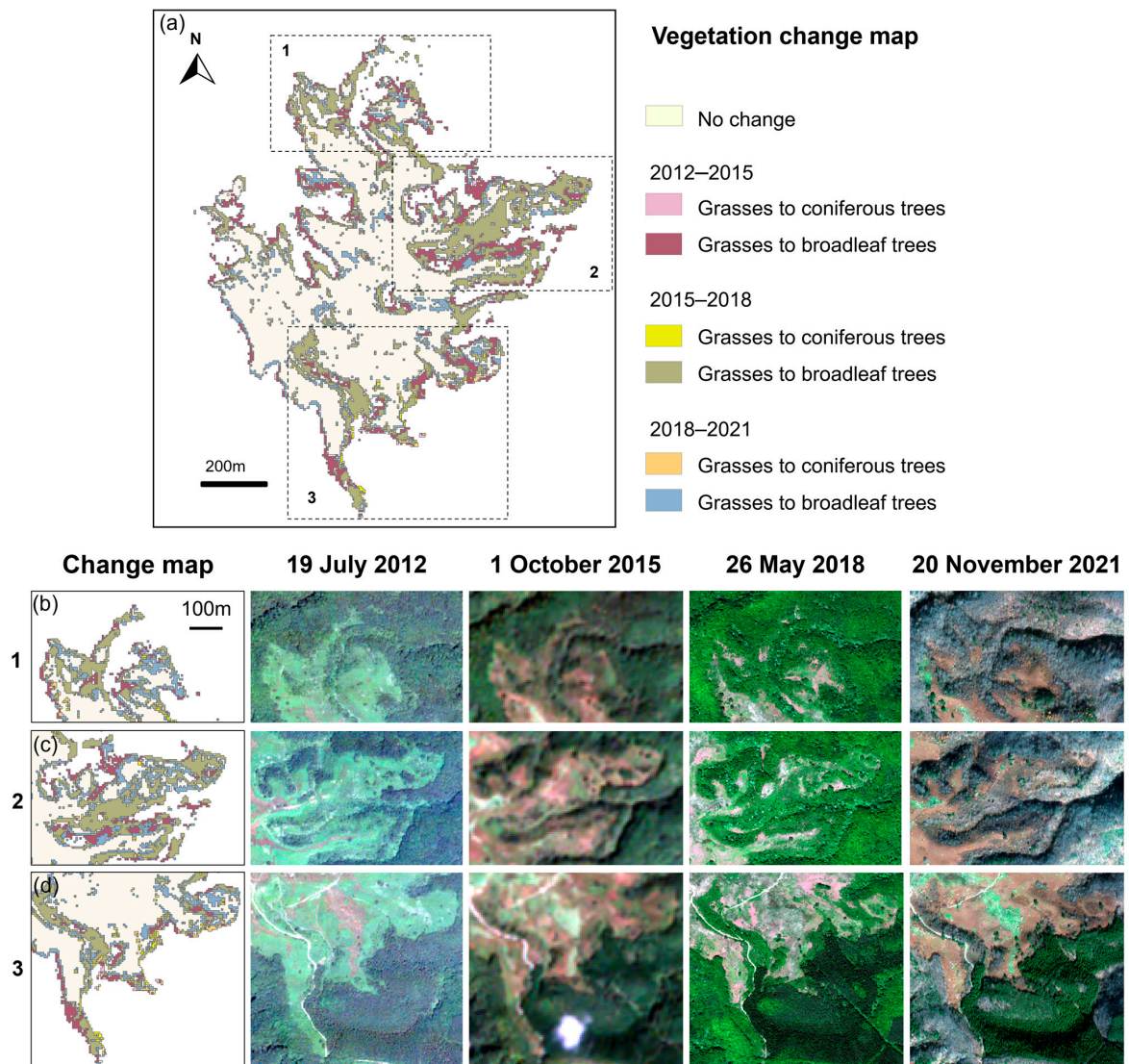
Figure 4. (**a**) Vegetation change map of the Rokkaku pasture. (**b**–**d**) are zoom-in views of the change map in (**a**) for case regions labeled as 1, 2, and 3, respectively. Each zoom-in view is a complication of the change map and true-color RGB images from four dates: 19 July 2012 (QuickBird, R: band 3; G: band 2; B: band 1), 1 October 2015 (SPOT-7, R: band 3; G: band 2; B: band 1), 26 May 2018 (WorldView-2, R: band 5; G: band 3; B: band 2), and 20 November 2021 (WorldView-2, R: band 5; G: band 3; B: band 2).
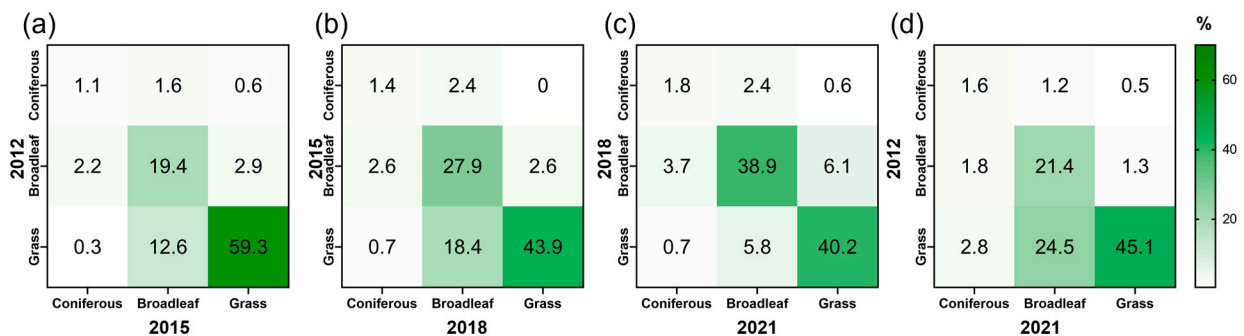

Figure 5. Heat map showing the percentage of vegetation change in the study area over four periods. (**a**) Change from 2012 to 2015, (**b**) from 2015 to 2018, (**c**) from 2018 to 2021, and (**d**) a comprehensive view of the change from 2012 to 2021. The color bar represents the percentage of change in vegetation.

3.4. Topographical Correlations with Vegetation Change

The elevation of the Rokkaku pasture ranges from 483 to 621 m, being lower toward the northeast and higher in the southwest (Figure 6a). Predominantly, the pasture is flat (<15°), with slopes becoming steeper near the boundaries (Figure 6b). The northeast-facing slopes are the most common (Figure 6c). Violin plots (Figure 6d–f) illustrate the distribution of vegetation changes from 2012 to 2021 with respect to elevation, slope, and aspect.
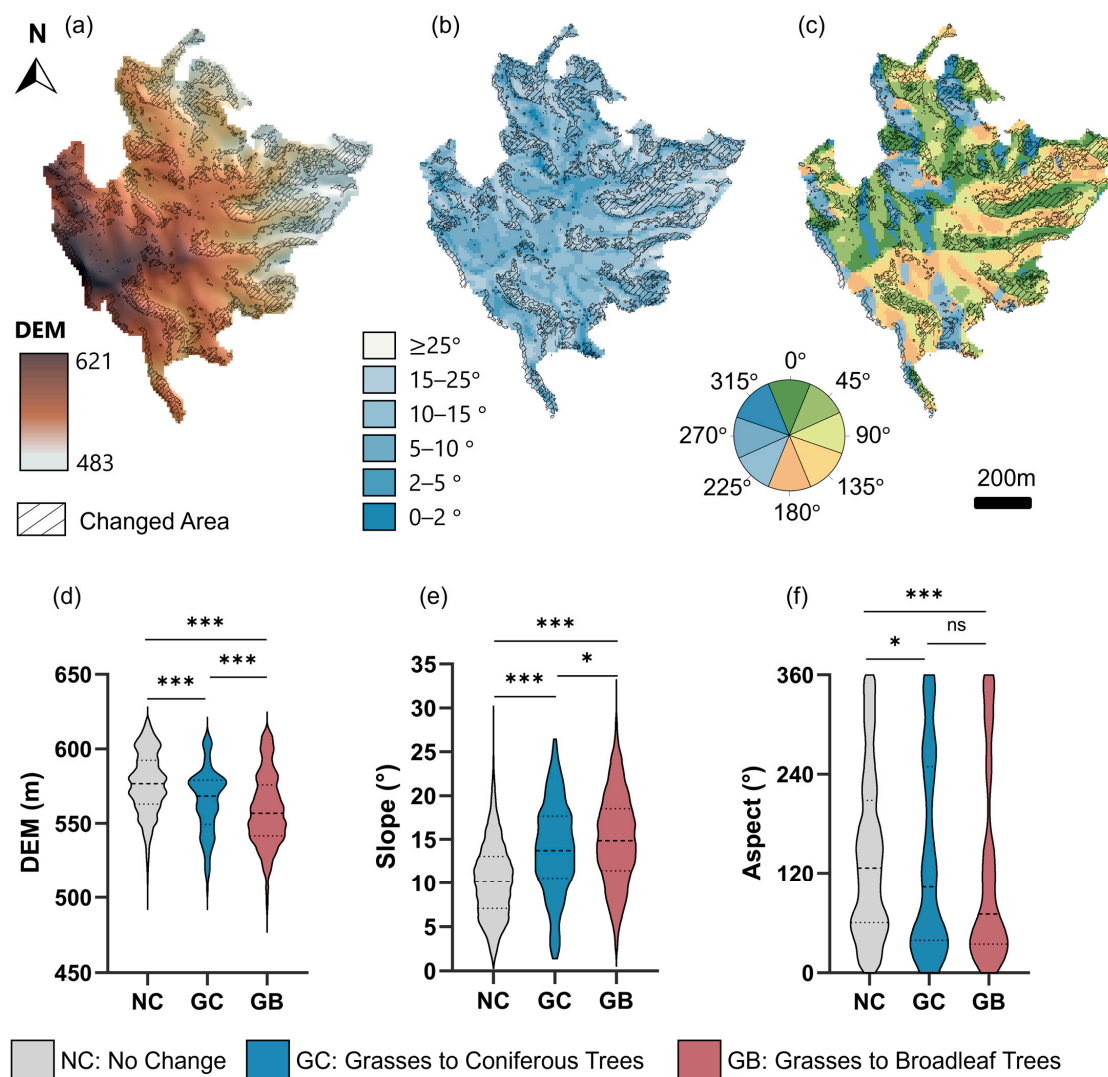

Figure 6. Relationships between topographic factors and vegetation change. (**a**) Elevation, (**b**) slope, and (**c**) aspect maps. Violin plots (**d–f**) representing the distribution of vegetation changes over the period from 2012 to 2021 in relation to elevation, slope, and aspect, respectively, based on the Kruskal–Wallis H test. Statistical significance was determined using the Dunn post-hoc test and is represented as follows: 'ns' for $p \geq 0.05$ (non-significant), * for $p < 0.05$, and *** for $p < 0.001$, with each decreasing *p*-value representing higher statistical significance.

3.4.1. Elevation

In terms of elevation and vegetation change, we observed a disparity between the means of each group with tighter clustering of data around their respective means. (Figure 6d). Dunn's post-hoc test confirmed statistical differences across all three groups ($p < 0.001$). The NC group exhibited the highest mean elevation at 576.8 m, while the GB group demonstrated the lowest mean at 559.0 m, indicating that vegetation change from grasses

to broadleaf trees tends to occur at slightly lower elevations than that of areas where no significant vegetation change is observed.

3.4.2. Slope

The distribution of the slope also differed significantly across the three groups (Figure 6e; $p < 0.05$). The mean values of slope degree for the changed groups (GB: 15.0° and GC: 13.9°) were greater than that of the group with no changes (10.3°). These areas of vegetation change, both in GB and GC, tended to be associated with steeper slopes than those of areas with no significant vegetation change.

3.4.3. Aspect

Regarding the relationship between aspect and vegetation change, we found statistically significant differences between NC and the other groups (Figure 6f; $p < 0.05$). However, the differences between the GB and NC groups were not statistically significant ($p \geq 0.05$). In the GB group, a notably denser data distribution below the mean indicated that a substantial proportion of this group associates with northeast-facing slopes within an aspect range of 22.5° to 67.5°. This distribution coincided with the most concentrated data values in the 25th percentile, at 34.4°. For the GC group, the statistical descriptors showed tendencies similar to those of the GB group. The data distribution was denser around the 25th percentile (39.1°), suggesting that regions where vegetation undergoes a transition from grasses to trees are predominantly situated on east- and northeast-facing slopes compared with the non-changing region.

4. Discussion

4.1. Comparison of Pasture Area Change between High- and Medium-Resolution Satellite Imagery

The application of optical remote sensing often encounters difficulties owing to obstructions from cloudy conditions, which can disrupt the acquisition of pertinent data from specific locations. In the present study, we noted disparities in the observation times of multi-temporal high-resolution satellite images. These inconsistencies might influence the outcomes of area change, particularly when considering seasonal changes in vegetation. The resolution of these images varied from 1.8 to 6 m. Conversely, medium-resolution imagery from sources such as Landsat-5/7/8 satellites is readily available and can be used selectively, although its 30-m multispectral resolution might not capture minute changes effectively, leading to errors from mixed pixels, especially in smaller regions, such as the Daishaku pasture. Time-series analyses of the Daishaku pasture revealed fluctuations around 0.5 ha attributable to these mixed pixel errors. Nevertheless, both Landsat and Sentinel-2 analyses yielded changing trends for pasture areas consistent with those from high-resolution satellite imagery (Figure 3). Landsat images are particularly advantageous for long-duration studies because of their extensive data archives. Using these archives, we confirmed that the pasture area remained consistent under regular grazing between 2007 and 2011. Furthermore, these archives provide images every May or June from 2011, allowing for continuous time-series observation of pasture area changes after grazing ceased. The Sentinel-2 series provides superior spatial resolution compared with that of Landsat, supplying images every May, June, or July from 2017 onward and facilitating continuous time-series observations of pasture area changes. Although its data are limited to the post-2017 period, Sentinel-2 is a suitable choice for those aiming to strike a balance between spatial detail and temporal scope in continuous monitoring. Therefore, despite their resolution-related shortcomings, medium-resolution satellite images remain crucial for land-cover categorization and change detection, providing trustworthy information. They are particularly valuable when high-resolution data are either unattainable or cost-prohibitive.

In studying ecosystems, such as grasslands or vegetation assessments, the amalgamation of high-resolution and readily sourced medium-resolution data, such as Landsat and Sentinel-2, is advantageous. Utilizing these multiscale datasets provides a comprehen-

sive perspective, promoting a thorough analysis and informed decision-making. Merging datasets can offset the constraints of one source with the advantages of another. For instance, while high-resolution images yield detailed spatial data, medium-resolution sources, such as Landsat, provide a broader time frame. This integrated approach effectively reduces data gaps and ensures sustained observations.

However, it is also essential to consider the limitations associated with varying resolutions. Even though high-resolution imagery provides detailed spatial data, it can have inconsistent observation times, which might lead to challenges in effectively capturing seasonal changes. The precision of maps and derived area estimates are shaped by the training data used for supervised classification, quality of the base imagery, and implemented methodologies. For a specific region, the accuracy and area estimates might vary based on the classification approach—whether it is per-pixel or object-based—or if there is an alteration in the imagery's spatial resolution [41].

4.2. Vegetation Change Process and Its Influences

4.2.1. Vegetation Changes and Human Intervention

High-resolution classification results and change maps showed that from 2012 to 2015, the area of the Rokkaku Pasture decreased from 66 to 57.2 ha (Figure 3a), primarily transitioning into broadleaf trees (Figure 4a). This transformation was most evident in the western portion of the narrow region on the southern edge, characterized by slopes steeper than 15°, facing west and northwest and at lower elevations (Figures 4d and 6a–c). This region Is surrounded by broadleaf trees to the west and coniferous trees to the east. Overall, during this period, the transition was mainly observed at the northern, eastern, and southern boundaries and in interspaces near trees, where the elevation was relatively lower than that in the west (Figures 4a and 6a). From 2015 to 2018, the area of the Rokkaku Pasture decreased from 57.2 to 41.9 ha (Figure 3a). Among the three distinct periods, the most pronounced alterations occurred during this period (Figure 4a). Notably, the narrow region on the northern edge, characterized by lower elevation and mainly facing northwest, underwent significant transitions from grasses to tree-dominated areas (Figures 4b and 6a,c). The adjacent boundaries exhibited similar transitions. Tree encroachment was particularly evident on the eastern side, which featured the lowest elevations and steeper slopes (>15°), facing north, east, and south (Figures 4c and 6a–c). Such encroachment was observed in the northwestern part of Region 3, with the transformation primarily occurring in areas facing northeast, with slope degrees greater than 15° (Figures 4d and 6b,c). The eastern part of the narrow region on the southern edge completely transformed into a tree-dominated area (Figure 4d). From 2018 to 2021, tree invasion was observed not only at the boundary between the pasture and forest but also within the pasture, predominantly surrounding the isolated woodlands (Figure 4a).

Temporal analysis of land cover classification revealed a substantial decline in the area of the Rokkaku Pasture from 2012 to 2022 (Figure 3a), a change correlated with grazing suspension after the Great East Japan Earthquake on 11 March 2011. Notably, from 2018 onwards, the area fluctuated between 41.9 and 42.1 ha, suggesting a period of relative stability (Figure 3). Therefore, it is vital to continue monitoring to better understand these dynamics. Certain variations could be attributed to misclassification errors. Upon the cessation of grazing activities, the effects of cattle grazing behavior and grassland management were effectively eliminated, facilitating the flourishing of tree seeds and transforming the previously grass-dominated area into a wooded region. In Japan's humid and warm temperate environment, human intervention is essential for maintaining grasslands [9,10]. These observations underscore the considerable influence of natural disasters and human intervention on landscape transformations. Current plant species richness is more strongly correlated with past rather than present habitat areas [42], further emphasizing the importance of historical land use in shaping current biodiversity. While there have been marked alterations in land cover, the Rokkaku Pasture exhibited remarkable stability after 2018. The underlying reasons for this resilience remain elusive. Therefore, a meticulous investi-

gation into the factors contributing to this resilience, coupled with continued monitoring, is imperative. Such research could potentially elucidate strategies pivotal for effective grassland conservation.

Overall, the transformation from grasses to trees occurred primarily along the southern, eastern, and northern boundaries, where diminishing grasses mainly transitioned into broadleaf trees. In contrast, the conversion from grasses to coniferous trees was markedly less prevalent. The climax vegetation is contingent on regional climatic conditions. In Japan's temperate and humid environment, broadleaf trees are hypothesized to constitute climax vegetation [43].

4.2.2. Role of Topography in Vegetation Changes

Changes in ecosystem boundaries result from the cumulative responses of individuals to local conditions encompassing microclimates along the biome transition zones [44]. A preference for eastern and northeastern slopes was observed in both the GC and GB groups, indicating that regions where vegetation transitioned from grasses to trees predominantly lie on slopes oriented toward the east and northeast. Differences in humidity and temperature owing to slope orientation create distinct ecological niches for plant species, thereby influencing the vegetation they support [45]. We observed shifts in vegetation from grasses to broadleaf trees, which were predominantly associated with steeper slope angles and slightly lower elevations compared with areas without vegetation change (Figure 6d,e). The higher mean slope angle for the "changed" groups also intimates that alterations in vegetation might be more prevalent or perceptible in areas with greater topographic variation. In addition, lower elevations can offer a more temperate climate, favoring tree growth [43]. This has been confirmed by studies showing higher seedling density and richness in moist, low-elevation valley habitats [46]. These observations suggest that topographic features, including elevation, slope angle, and aspect, play significant roles in shaping vegetation changes. These features interact with the climate and other environmental factors, thereby shaping the relationship between topographic characteristics and vegetation types [47]. Detailed terrain analysis is required to fully understand this relationship in future research.

4.2.3. Influence of Wind, Seed Dispersal, and Forest Canopy on Vegetation Changes

The prevailing wind direction changes seasonally: westward in spring and winter, east–southeast and east in summer and early autumn, and west–northwest in late autumn [28]. The forest canopy surrounding the western part of the southern edge, where there is a noticeable encroachment of broadleaf trees (Figure 4d), is bordered by broadleaf trees to the west and coniferous trees to the east. Given the dominant northwesterly winds during autumn, broadleaf seeds were mainly dispersed southeastward. However, in most other areas, no relationship was observed between wind direction and vegetation changes.

The forest canopy around the Rokkaku pasture mainly consists of *F. crenata*, which often forms clusters. A noticeable encroachment of these trees into pasture, especially on hillside slopes, was observed (Figure 6a). The observed encroachment on hillside slopes may be attributed to the clustering characteristics of *F. crenata*. One limitation of our study is that, although significant encroachments of broadleaf trees into the pasture were identified, we did not provide a detailed classification of other tree species. A comprehensive understanding of tree species and their interactions would provide a clearer understanding of the area's ecological transitions. Moreover, our research did not deeply investigate other influential factors, such as soil characteristics, that may affect vegetation dynamics. Future research would be enriched by a thorough tree classification and analysis to comprehensively understand land changes.

4.2.4. Comparative Analysis of Woody Encroachment

In several studies, a discernable trend of woody encroachment into herbaceous terrains has been observed, especially in regions experiencing warmer and wetter climates. For instance, Liu et al. [21] observed a significant trend in transitional zones such as forest

and steppe ecotones, mountain forest margins, and extension areas. The authors mainly attributed this to climate warming in places where active fires were suppressed. Simultaneously, there has been a resurgence of grass in regions under milder warming and desiccation trends, where human disturbances such as fire regimes and population density have shown a more significant influence than the effects of climate warming. Contrastingly, the Rokkaku pasture in our study showed an accelerated rate of woody encroachment, influenced more strongly by the absence of human activity (e.g., cattle grazing and grassland management) than by climatic factors alone. Furthermore, Song et al. [48] showcased a net increase in tree cover in tropical regions, with 60% of all land changes directly tied to human action. Together with our results, these findings highlight the intricate balance between natural phenomena and human interventions in determining the fate of grassland ecosystems. While the specifics of human interventions may vary, a common thread is the transformation of grasslands due to woody encroachment, which is taking place at diverse rates and scales. These evolving dynamics can have far-reaching consequences, influencing biodiversity, soil health, and even water resources. To navigate this landscape transformation, more comprehensive research is essential, aiming to understand the long-term impacts and craft region-specific management strategies.

4.3. Limitations of This Study and Directions for Future Research

Despite our comprehensive approach to analyzing changes in pasture areas and vegetation dynamics, this study has several limitations that should be acknowledged. The primary limitation is the inadequacy of high-resolution satellite images. We were unable to find appropriate images in some years, such as 2010 and 2011. Optical remote sensing data are often compromised by cloud cover, leading to data gaps, especially in cloud-prone regions. Future research could benefit from the integration of synthetic aperture radar data analysis, which can penetrate cloud cover and provide imaging capabilities during both day and night, potentially enhancing the observation of pasture areas. Another limitation is the classification methodology. Our study utilized the traditional maximum likelihood classification technique for interpreting satellite data. While this method is widely adopted, the choice of classification method and the training data used for supervised classification can influence the outcomes. Furthermore, our study provides an analysis of the impact of topography on vegetation changes but does not extensively explore other influential variables such as soil characteristics, wildlife activities, and microclimatic conditions. These factors could significantly impact vegetation dynamics and landscape changes.

Another important aspect to consider is the context of our study area, particularly in light of the Great East Japan Earthquake and the subsequent Fukushima Daiichi Nuclear Power Plant incident. These events have significantly altered human activities in the region, which in turn have had a profound impact on the natural environment. These changes underscore the need for continued long-term monitoring to understand the evolving dynamics of the landscape. Employing both paid and free satellite imagery can be instrumental in this regard, providing a comprehensive view over time and aiding in the assessment of the long-term effects of such major events on pasture areas and vegetation dynamics. Our study, which focused on the Rokkaku Pasture, also indicates the need for further analysis of other pasture areas affected by the Great East Japan Earthquake to improve the generalizability of our conclusions. Future research should aim to address these gaps by incorporating a more diverse range of data sources, employing varied analytical methods, and extending the scope to include additional environmental and anthropogenic factors.

5. Conclusions

This study revealed a significant transformation in the land cover of a pasture area where grazing ceased since 2011, as evidenced by multiscale high-resolution satellite imagery and Landsat-5/7/8 and Sentinel-2 imagery. Notably, both high- and medium-resolution satellites yielded congruent area measurements. The high-resolution imagery elucidated detailed spatial changes, whereas the medium-resolution imagery offered a

broader temporal perspective. The pasture area showed a significant reduction of more than 35% following the voluntary cessation of grazing after the 2011 earthquake. In contrast, pastures that remained under continuous grazing demonstrated stability. The reduction in pasture area was predominantly attributed to broadleaf tree encroachment. The eastern side, characterized by its lower elevation and steeper slopes facing north, east, and south, was particularly marked by tree encroachment. This shift from grasses to broadleaf trees appears to have been influenced by both natural and anthropogenic factors, reflecting the interplay between ecological dynamics and human intervention. This study reaffirms the utility of both high- and medium-resolution satellite imagery for land-cover classification and change detection. These tools provide invaluable insights into the dynamic and complex nature of terrestrial ecosystems and emphasize the importance of continued monitoring for sustainable land management and biodiversity conservation. In future research, a detailed terrain analysis coupled with tree classification could provide deeper insights into land cover change.

References

1. White, R.P.; Murray, S.; Rohweder, M. *Pilot Analysis of Global Ecosystems: Grassland Ecosystems*; World Resources Institute: Washington, DC, USA, 2000.
2. Gibson, D.J. *Grasses and Grassland Ecology*; Oxford University Press: Oxford, UK, 2009. ISBN 9780191546099.
3. Bardgett, R.D.; Bullock, J.M.; Lavorel, S.; Manning, P.; Schaffner, U.; Ostle, N.; Chomel, M.; Durigan, G.; Fry, E.L.; Johnson, D.; et al. Combatting Global Grassland Degradation. *Nat. Rev. Earth Environ.* **2021**, *2*, 720–735. [CrossRef]
4. Zhang, C.; Dong, Q.; Chu, H.; Shi, J.; Li, S.; Wang, Y.; Yang, X. Grassland Community Composition Response to Grazing Intensity under Different Grazing Regimes. *Rangel. Ecol. Manag.* **2018**, *71*, 196–204. [CrossRef]
5. Milchunas, D.G.; Lauenroth, W.K. Quantitative Effects of Grazing on Vegetation and Soils over a Global Range of Environments. *Ecol. Monogr.* **1993**, *63*, 327–366. [CrossRef]
6. McSherry, M.E.; Ritchie, M.E. Effects of Grazing on Grassland Soil Carbon: A Global Review. *Global Change Biol.* **2013**, *19*, 1347–1357. [CrossRef]
7. Ogura, J. Changes of grassland area in Japan. *Bull Kyoto Seika Univ.* **2006**, *30*, 159–172. (In Japanese)
8. The National Biodiversity Strategy and Action Plan (NBSAP) 2012–2020 Japan. Available online: https://www.env.go.jp/press/ files/en/528.pdf (accessed on 17 May 2023).
9. Ushimaru, A.; Uchida, K.; Suka, T. Grasslands of the World. In *Grasslands of the World: Diversity, Management and Conservation*; Squires, V.R., Dengler, J., Hua, L., Feng, H., Eds.; Routledge: Abingdon, UK, 2018; pp. 197–218. ISBN 9781315156125.
10. Numata, M.; Itow, A.M.; Itow, D. Natural and Semi-Natural Vegetation in Japan. *Blumea Biodivers. Evol. Biogeogr. Plants* **1972**, *20*, 435–496.
11. Ali, I.; Cawkwell, F.; Dwyer, E.; Barrett, B.; Green, S. Satellite Remote Sensing of Grasslands: From Observation to Management. *J. Plant Ecol.* **2016**, *9*, 649–671. [CrossRef]
12. Leeuw, J.D.; Georgiadou, Y.; Kerle, N.; Gier, A.D.; Inoue, Y.; Ferwerda, J.; Smies, M.; Narantuya, D. The Function of Remote Sensing in Support of Environmental Policy. *Remote Sens.* **2010**, *2*, 1731–1750. [CrossRef]
13. Asam, S.; Klein, D.; Dech, S. Estimation of Grassland Use Intensities Based on High Spatial Resolution LAI Time Series. *Int. Arch. Photogramm. Remote Sens. Spatial Inf. Sci.* **2015**, *40*, 285–291. [CrossRef]
14. Stumpf, F.; Schneider, M.K.; Keller, A.; Mayr, A.; Rentschler, T.; Meuli, R.G.; Schaepman, M.; Liebisch, F. Spatial Monitoring of Grassland Management Using Multi-Temporal Satellite Imagery. *Ecol. Indic.* **2020**, *113*, 106201. [CrossRef]

15. Halabuk, A.; Mojses, M.; Halabuk, M.; David, S. Towards Detection of Cutting in Hay Meadows by Using of NDVI and EVI Time Series. *Remote Sens.* **2015**, *7*, 6107–6132. [CrossRef]

16. Edirisinghe, A.; Hill, M.J.; Donald, G.E.; Hyder, M. Quantitative Mapping of Pasture Biomass Using Satellite Imagery. *Int. J. Remote Sens.* **2011**, *32*, 2699–2724. [CrossRef]

17. Lange, M.; Feilhauer, H.; Kühn, I.; Doktor, D. Mapping Land-Use Intensity of Grasslands in Germany with Machine Learning and Sentinel-2 Time Series. *Remote Sens. Environ.* **2022**, *277*, 112888. [CrossRef]

18. Kokaly, R.F.; Despain, D.G.; Clark, R.N.; Livo, K.E. Mapping Vegetation in Yellowstone National Park Using Spectral Feature Analysis of AVIRIS Data. *Remote Sens. Environ.* **2003**, *84*, 437–456. [CrossRef]

19. Filippa, G.; Cremonese, E.; Galvagno, M.; Bayle, A.; Choler, P.; Bassignana, M.; Piccot, A.; Poggio, L.; Oddi, L.; Gascoin, S.; et al. On the Distribution and Productivity of Mountain Grasslands in the Gran Paradiso National Park, NW Italy: A Remote Sensing Approach. *Int. J. Appl. Earth Obs.* **2022**, *108*, 102718. [CrossRef]

20. Wang, J.; Xiao, X.; Qin, Y.; Dong, J.; Geissler, G.; Zhang, G.; Cejda, N.; Alikhani, B.; Doughty, R.B. Mapping the Dynamics of Eastern Redcedar Encroachment into Grasslands during 1984–2010 through PALSAR and Time Series Landsat Images. *Remote Sens. Environ.* **2017**, *190*, 233–246. [CrossRef]

21. Liu, X.; Feng, S.; Liu, H.; Ji, J. Patterns and Determinants of Woody Encroachment in the Eastern Eurasian Steppe. *Land Degrad. Dev.* **2021**, *32*, 3536–3549. [CrossRef]

22. Belward, A.S.; Skøien, J.O. Who Launched What, When and Why; Trends in Global Land-Cover Observation Capacity from Civilian Earth Observation Satellites. *ISPRS J. Photogramm. Remote Sens.* **2015**, *103*, 115–128. [CrossRef]

23. Agriculture, Forestry and Fisheries Research Council (AFFRC). Distribution Map of Radioactive Material Concentration in Agricultural Soil. Available online: https://www.affrc.maff.go.jp/docs/press/pdf/110830-06.pdf (accessed on 21 April 2023). (In Japanese)

24. Ministry of Agriculture, Forestry and Fisheries (MAFF). Information on Measures for Reduction of Radionuclide Contamination of Agricultural Produce after the Accident at Fukushima Daiichi Nuclear Power Plant in Japan. Available online: https://www.maff.go.jp/e/policies/food_safety/emer/attach/pdf/202209_summary.pdf (accessed on 26 April 2023).

25. Harada, I.; Hara, K.; Park, J.; Asanuma, I.; Tomita, M.; Hasegawa, D.; Short, K.; Fujihara, M. Monitoring of Rapid Land Cover Changes in Eastern Japan Using Terra/MODIS Data. *Int. Arch. Photogramm. Remote Sens. Spatial Inf. Sci.* **2015**, *40*, 403–408. [CrossRef]

26. Ishihara, M.; Tadono, T. Land Cover Changes Induced by the Great East Japan Earthquake in 2011. *Sci. Rep.* **2017**, *7*, 45769. [CrossRef] [PubMed]

27. Hirayama, H.; Tomita, M.; Sharma, R.C.; Hara, K. Land-Cover Maps Using Multiple Classifier System for Post-Disaster Landscape Monitoring. *Int. Arch. Photogramm. Remote Sens. Spatial Inf. Sci.* **2019**, *42*, 139–142. [CrossRef]

28. Historical Weather Data by Japan Meteorological Agency. Available online: https://www.data.jma.go.jp/obd/stats/etrn/index.php?prec_no=34&block_no=0243&year=&month=&day=&view= (accessed on 30 May 2023). (In Japanese)

29. Yonezawa, C.; Ogura, S.; Inoue, S.; Sasaki, S.; Namiwa, F.; Saito, G. Area and gradient estimation on grassland in Field Science Center. *Bull. Integr. Field Sci. Center* **2013**, *28*, 21–23. (In Japanese)

30. Goody, R.M.; Yung, Y.L. *Atmospheric Radiation: Theoretical Basis*; Oxford University Press: New York, NY, USA, 1989.

31. Wulder, M.A.; Ortlepp, S.M.; White, J.C.; Maxwell, S. Evaluation of Landsat-7 SLC-off Image Products for Forest Change Detection. *Can. J. Remote Sens.* **2008**, *34*, 93–99. [CrossRef]

32. Bradley, B.A. Remote Detection of Invasive Plants: A Review of Spectral, Textural and Phenological Approaches. *Biol. Invasions* **2014**, *16*, 1411–1425. [CrossRef]

33. Katoh, M. Classifying Tree Species in a Northern Mixed Forest Using High-Resolution IKONOS Data. *J. For. Res.* **2004**, *9*, 7–14. [CrossRef]

34. Pu, R.; Liu, D. Segmented Canonical Discriminant Analysis of in Situ Hyperspectral Data for Identifying 13 Urban Tree Species. *Int. J. Remote Sens.* **2011**, *32*, 2207–2226. [CrossRef]

35. Theil, H. A Rank-Invariant Method of Linear and Polynomial Regression Analysis. *Indag. Math.* **1950**, *12*, 173.

36. Sen, P.K. Estimates of the Regression Coefficient Based on Kendall's Tau. *J. Am. Stat. Assoc.* **1968**, *63*, 1379–1389. [CrossRef]

37. Kendall, M.G. *Rank Correlation Methods*; C. Griffin: London, UK, 1948.

38. Mann, H.B. Nonparametric Tests Against Trend. *Econometrica* **1945**, *13*, 245–259. [CrossRef]

39. Kruskal, W.H.; Wallis, W.A. Use of Ranks in One-Criterion Variance Analysis. *J. Am. Stat. Assoc.* **1952**, *47*, 583. [CrossRef]

40. Dunn, O.J. Multiple Comparisons Using Rank Sums. *Technometrics* **1964**, *6*, 241. [CrossRef]

41. Olofsson, P.; Foody, G.M.; Herold, M.; Stehman, S.V.; Woodcock, C.E.; Wulder, M.A. Good Practices for Estimating Area and Assessing Accuracy of Land Change. *Remote Sens. Environ.* **2014**, *148*, 42–57. [CrossRef]

42. Krauss, J.; Bommarco, R.; Guardiola, M.; Heikkinen, R.K.; Helm, A.; Kuussaari, M.; Lindborg, R.; Öckinger, E.; Pärtel, M.; Pino, J.; et al. Habitat Fragmentation Causes Immediate and Time-delayed Biodiversity Loss at Different Trophic Levels. *Ecol. Lett.* **2010**, *13*, 597–605. [CrossRef]

43. Harada, I.; Hara, K.; Tomita, M.; Short, K.; Park, J. Monitoring Landscape Changes in Japan Using Classification of Modis Data Combined with a Landscape Transformation Sere (LTS) Model. *J. Landsc. Ecol.* **2015**, *7*, 23–38. [CrossRef]

44. Oliveras, I.; Malhi, Y. Many Shades of Green: The Dynamic Tropical Forest–Savannah Transition Zones. *Philos. Trans. R. Soc. B Biol. Sci.* **2016**, *371*, 20150308. [CrossRef] [PubMed]

45. Farzam, M.; Ejtehadi, H. Effects of Drought and Slope Aspect on Canopy Facilitation in a Mountainous Rangeland. *J. Plant Ecol.* **2016**, *9*, rtw070. [CrossRef]
46. Jin, Y.; Russo, S.E.; Yu, M. Effects of Light and Topography on Regeneration and Coexistence of Evergreen and Deciduous Tree Species in a Chinese Subtropical Forest. *J. Ecol.* **2018**, *106*, 1634–1645. [CrossRef]
47. Holland, P.G.; Steyn, D.G. Vegetational Responses to Latitudinal Variations in Slope Angle and Aspect. *J. Biogeogr.* **1975**, *2*, 179. [CrossRef]
48. Song, X.-P.; Hansen, M.C.; Stehman, S.V.; Potapov, P.V.; Tyukavina, A.; Vermote, E.F.; Townshend, J.R. Global Land Change from 1982 to 2016. *Nature* **2018**, *560*, 639–643. [CrossRef]